Supporting Information for

Ultrafine Pt Nanoparticle-Decorated 3D Hybrid Architectures Built from Reduced Graphene Oxide and MXene Nanosheets for Methanol Oxidation

Cuizhen Yang, Quanguo Jiang, Weihua Li,* Haiyan He, Lu Yang, Zhiyong Lu, and Huajie Huang*

*Address correspondence to huanghuajie@hhu.edu.cn, liweihua3@mail.sysu.edu.cn

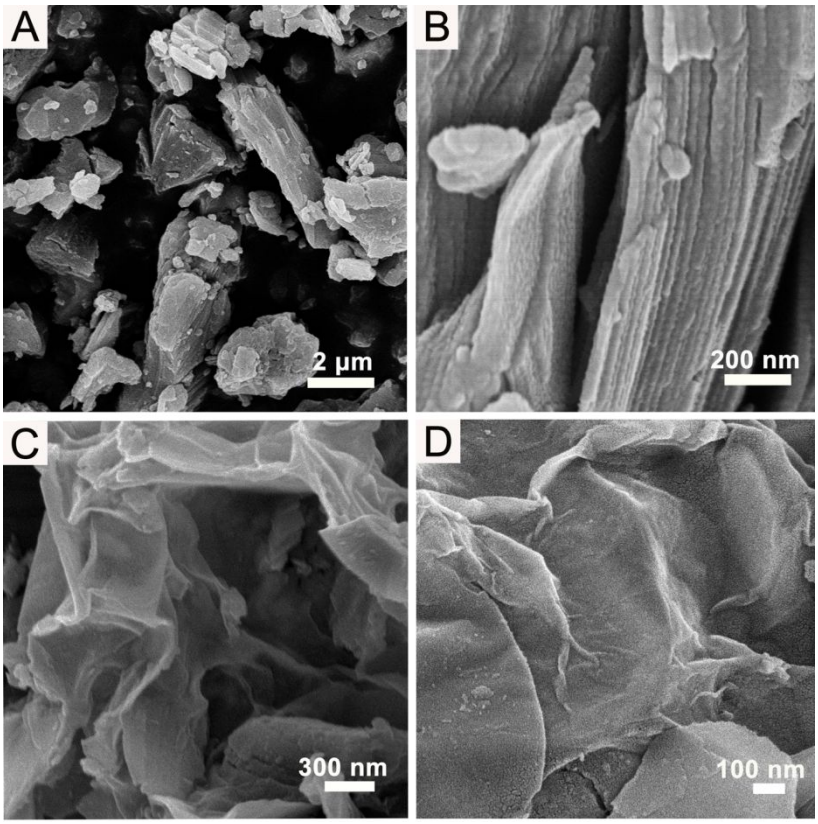

Figure S1. Representative SEM images of (A,B) Ti_3AlC_2 powders and (C,D) $Ti_3C_2T_x$ nanosheets, respectively, revealing the 2D lamellar structure of $Ti_3C_2T_x$ nanosheets.

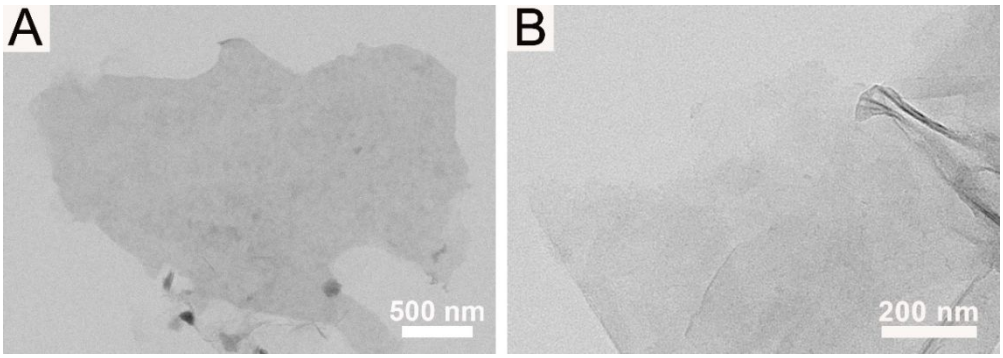

Figure S2. Typical TEM images of $Ti_3C_2T_x$ nanosheets show their ultrathin and transparent nature.

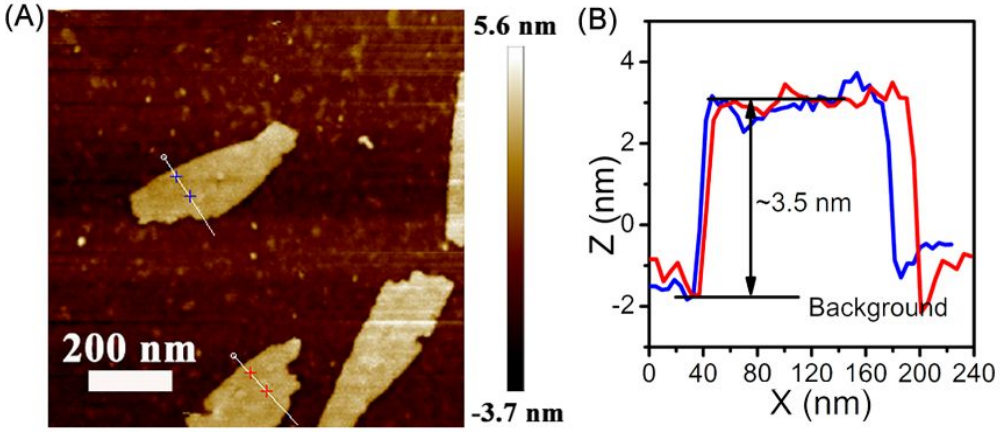

Figure S3. (A) Representative AFM image of the $Ti_3C_2T_x$ nanosheets. (B) The thickness analysis along the white lines discloses that the uniform thickness of the $Ti_3C_2T_x$ nanosheets is about 3.5 nm.

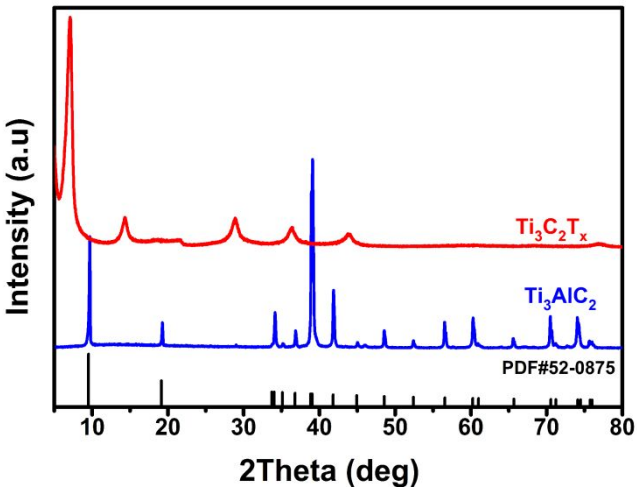

Figure S4. The XRD patterns of Ti_3AlC_2 powders and $Ti_3C_2T_x$ nanosheets, indicating the successful exfoliation of bulk Ti_3AlC_2 into $Ti_3C_2T_x$ nanosheets.

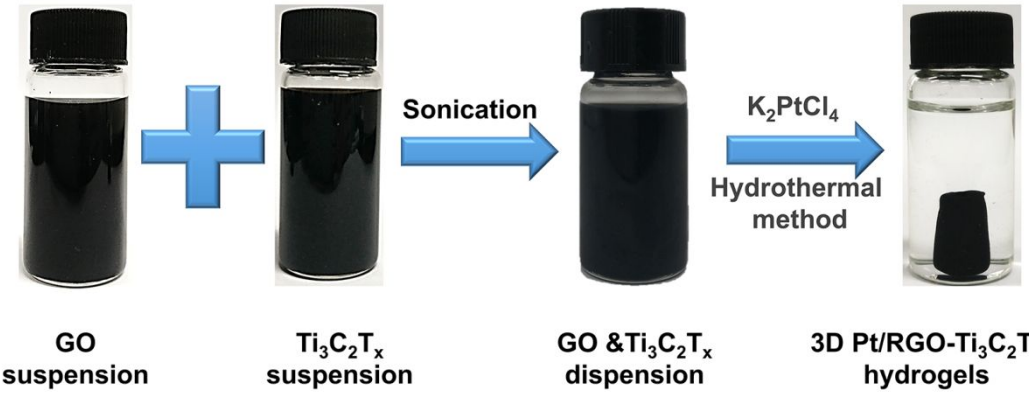

Figure S5. The synthetic process for the 3D Pt/RGO-$Ti_3C_2T_x$ hydrogels. It includes: (1) mixture GO and $Ti_3C_2T_x$ suspension via an ultrasonic treatment; (2) formation of 3D Pt/RGO-$Ti_3C_2T_x$ hydrogel through a solvothermal reaction.

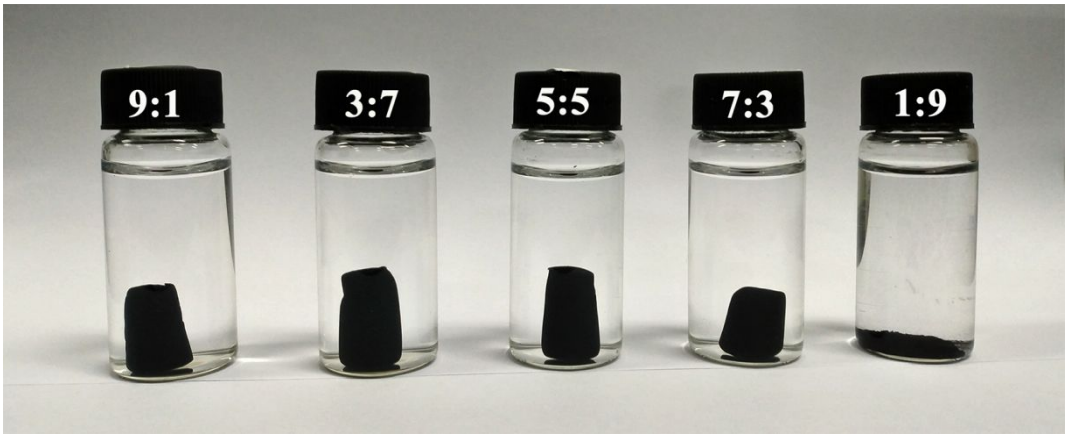

Figure S6. The digital photographs of the 3D Pt/RGO-$Ti_3C_2T_x$ hydrogels with varying RGO/$Ti_3C_2T_x$ ratios. It is found that a high $Ti_3C_2T_x$ content (>90 wt.%) will hinder the connection between GO nanosheets, thus making it difficult to obtain the 3D porous architectures.

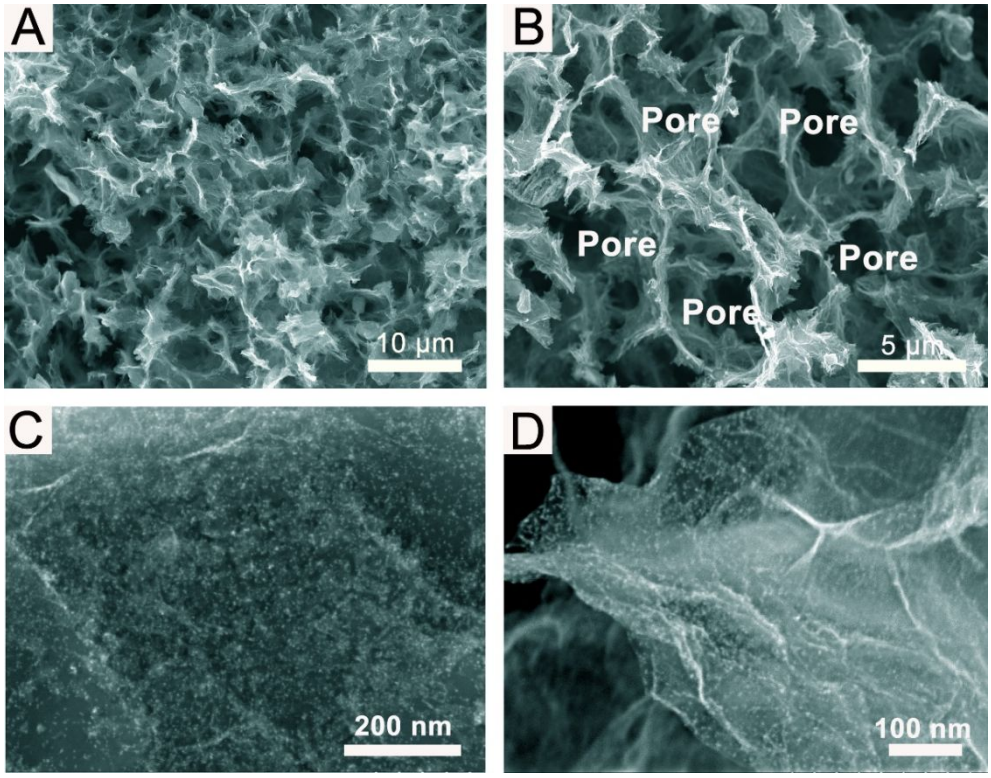

Figure S7. FE-SEM images of the 3D Pt/RGO-$Ti_3C_2T_x$ architecture at different magnifications. (A, B) Low-magnification FE-SEM images indicate that the material has numerous well-defined macropores. (C, D) High-magnification FE-SEM images

focused on $Ti_3C_2T_x$ and graphene regions, respectively, showing a uniform distribution of Pt NPs on both $Ti_3C_2T_x$ and graphene surfaces.

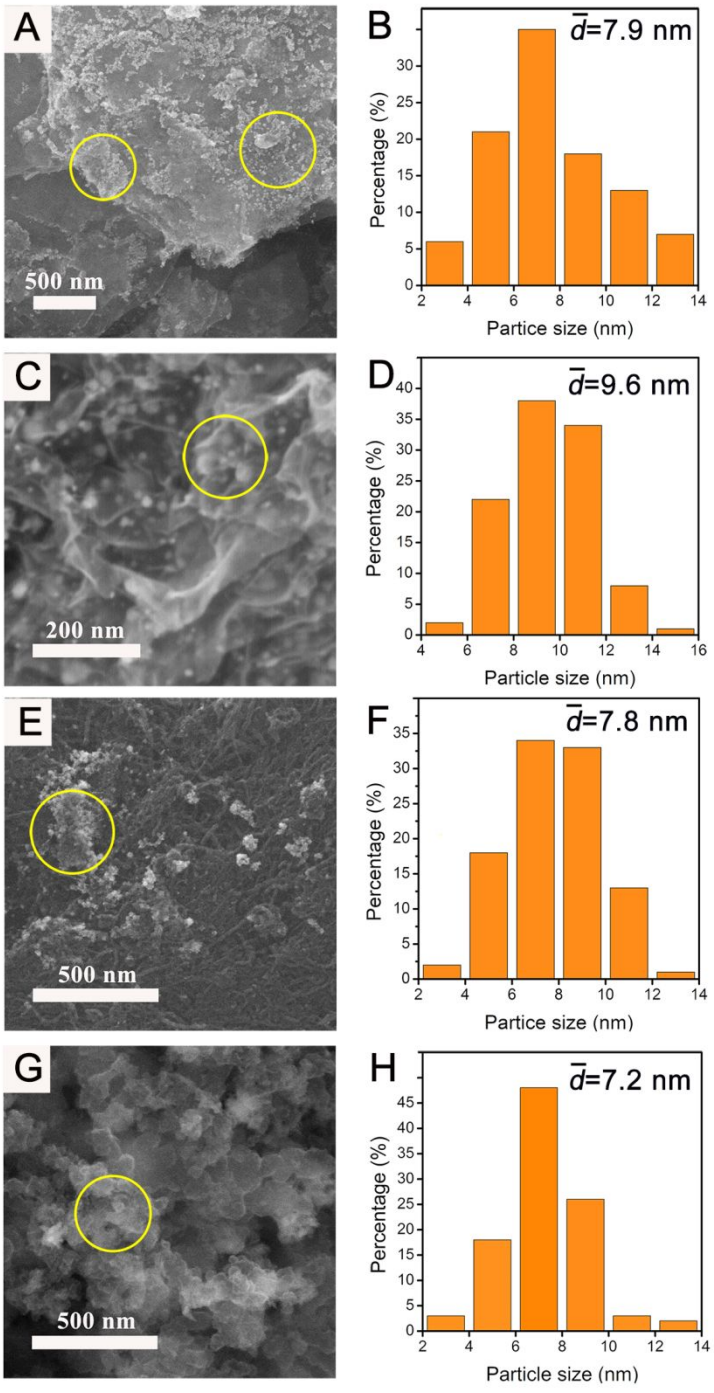

Figure S8. FE-SEM images and Pt particle size distribution of (A, B) Pt/$Ti_3C_2T_x$, (C, D) Pt/RGO, (E, F) Pt/CNT, and (G, H) Pt/C, respectively, revealing that Pt NPs are easy to form aggregates in these samples, as pointed out by the circles.

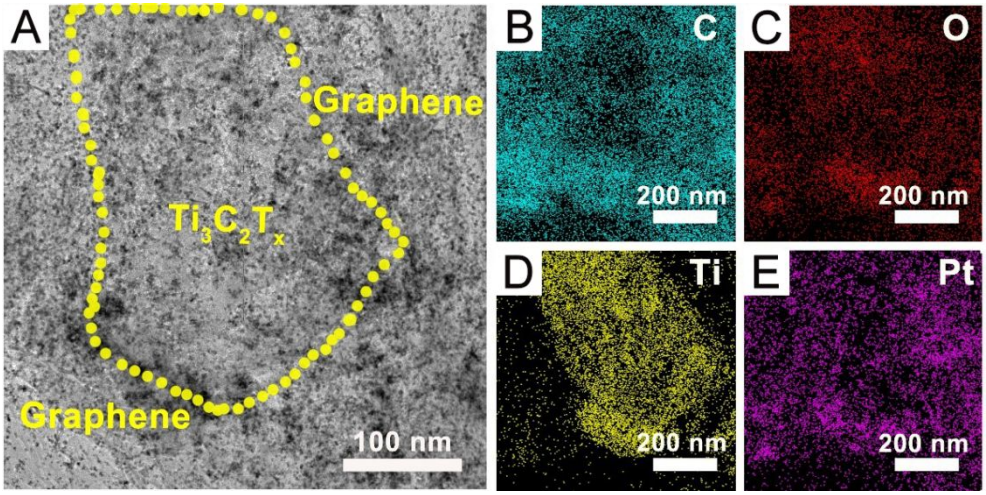

Figure S9. (A) TEM image of the Pt/RGO-$Ti_3C_2T_x$ architecture and the corresponding elemental mapping images of (B) C, (C) O, (D) Ti, and (E) Pt elements, demonstrating that the 2D $Ti_3C_2T_x$ nanosheets are confined into the 3D graphene networks.

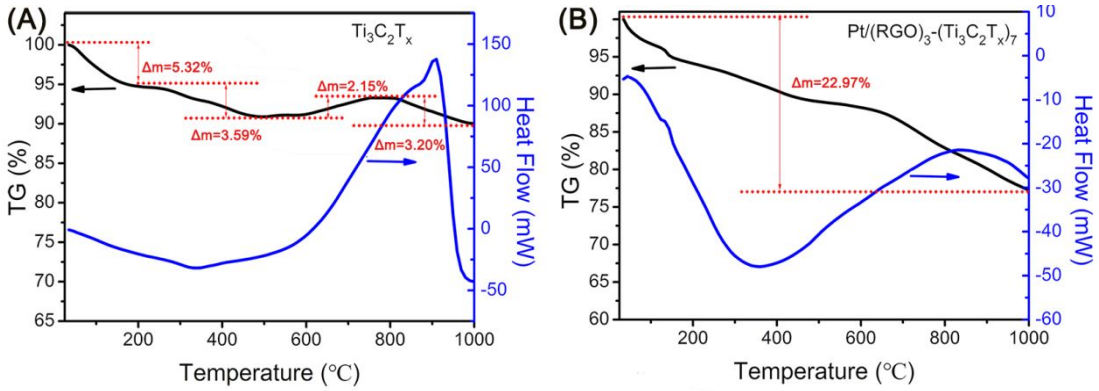

Figure S10. TG and DSC curves of (A) $Ti_3C_2T_x$ and (B) $Pt/(RGO)_3-(Ti_3C_2T_x)_7$ from room temperature to 1000 ℃ in argon atmosphere.

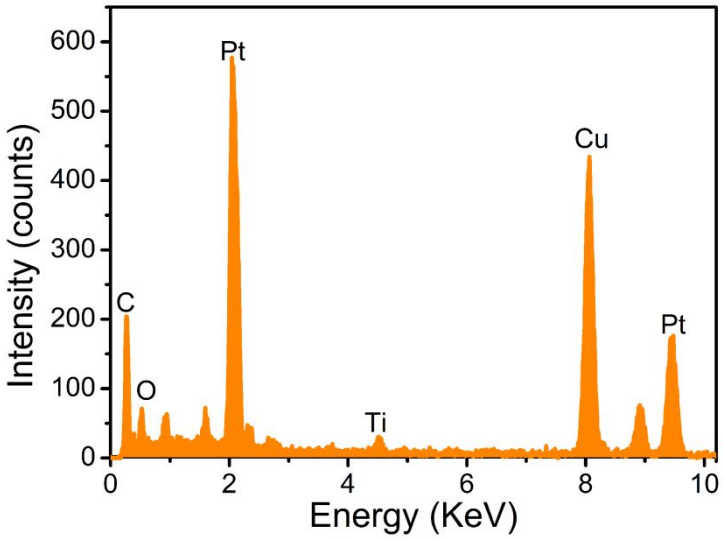

Figure S11. EDX spectrum of the 3D Pt/RGO-$Ti_3C_2T_x$ architecture confirms the co-existence of C, O, Ti and Pt components in the material. Since the sample was held on a Cu grid, Cu peaks were also detected.

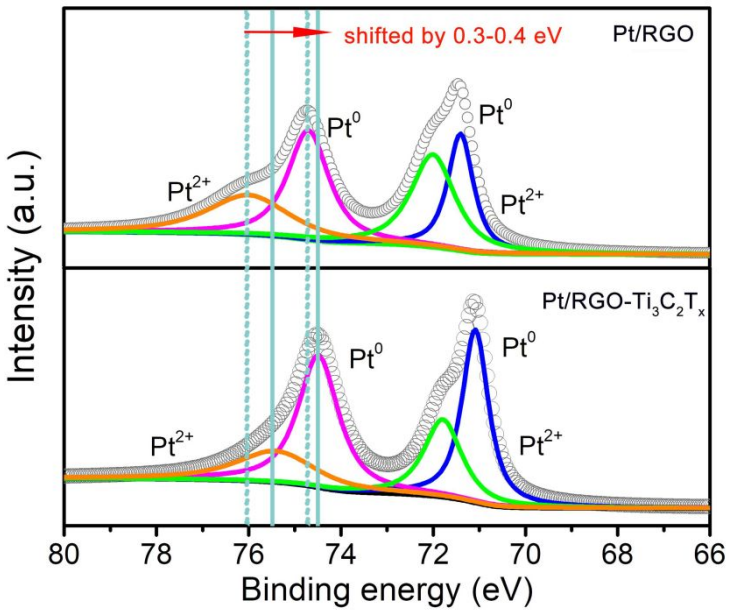

Figure S12. Pt 4f spectra of Pt/RGO-$Ti_3C_2T_x$ and Pt/RGO samples, showing that the binding energies for both metallic Pt and Pt^{2+} peaks of Pt/RGO-$Ti_3C_2T_x$ are shifted negatively compared with those of Pt/RGO.

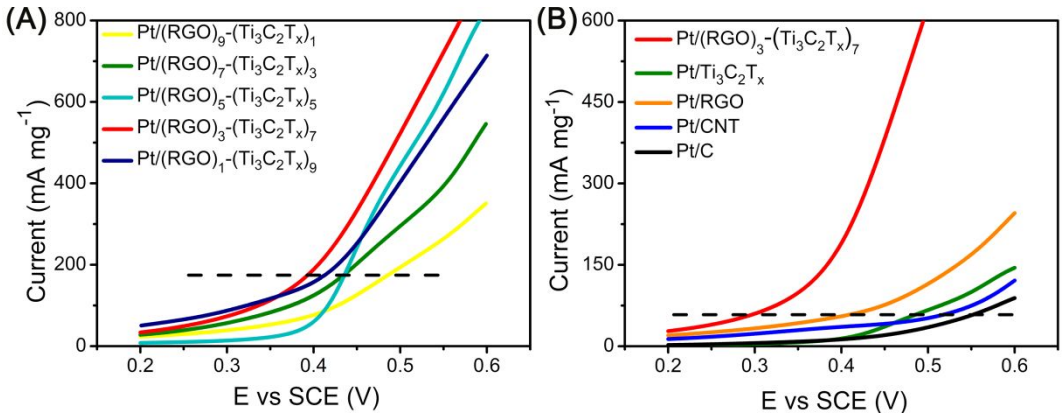

Figure S13. Linear sweep voltammetrys of (A) the Pt/RGO-$Ti_3C_2T_x$ architectures with varying RGO/$Ti_3C_2T_x$ ratios, and (B) Pt/$(RGO)_3$-$(Ti_3C_2T_x)_7$, Pt/RGO, Pt/$Ti_3C_2T_x$, Pt/CNT and Pt/C in 0.5 M H_2SO_4 solution at 50 mV s^{-1}, showing that the methanol oxidation reaction is much easier to take place on the Pt/$(RGO)_3$-$(Ti_3C_2T_x)_7$ electrode.

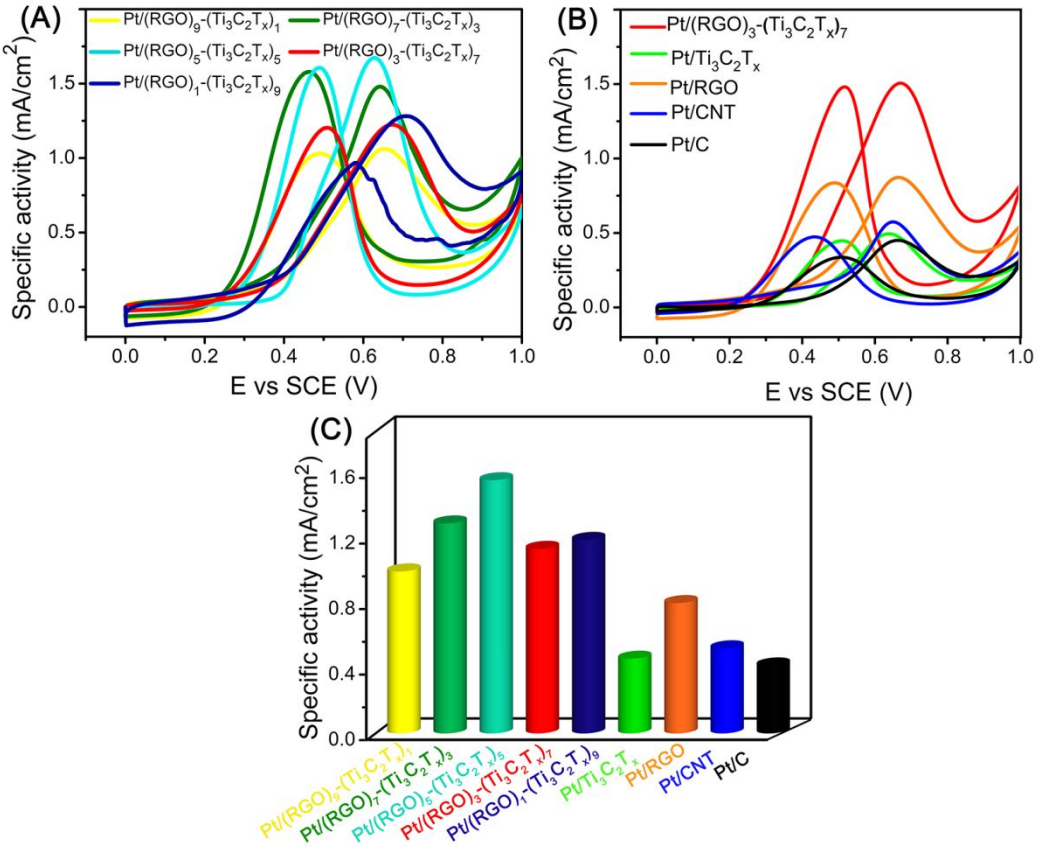

Figure S14. ECSA-normalized CV curves of (A) the Pt/RGO-$Ti_3C_2T_x$ architectures

with varying RGO/$Ti_3C_2T_x$ ratios, and (B) Pt/$(RGO)_3$-$(Ti_3C_2T_x)_7$, Pt/RGO, Pt/$Ti_3C_2T_x$, Pt/CNT and Pt/C. (C) Specific activities for different catalysts, confirming that the Pt/RGO-$Ti_3C_2T_x$ electrodes have much higher specific activities in comparison with the reference electrodes.

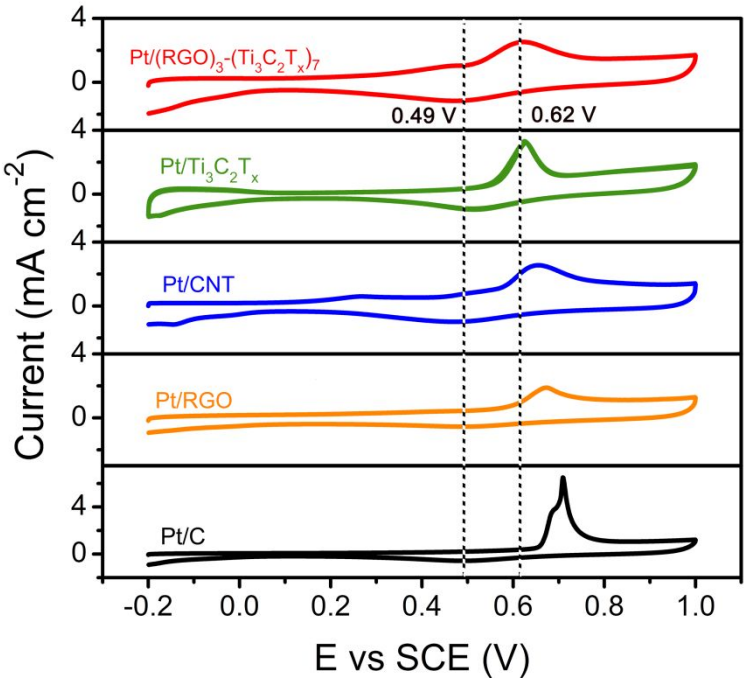

Figure S15. CO stripping voltammograms for Pt/$(RGO)_3$-$(Ti_3C_2T_x)_7$, Pt/$Ti_3C_2T_x$, Pt/CNT, Pt/RGO, and Pt/C catalysts tested in 0.5 M H_2SO_4 solution at a scan rate of 50 mV s^{-1}, suggesting that Pt/$(RGO)_3$-$(Ti_3C_2T_x)_7$ has the best anti-poisoning ability.

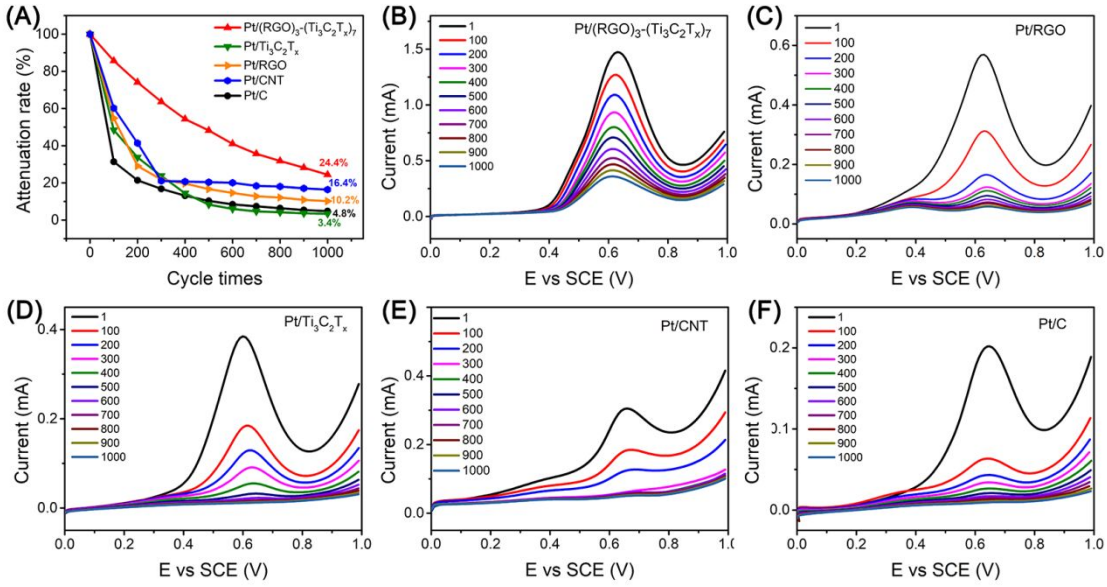

Figure S16. The stability behaviors of different catalysts toward methanol oxidation. (A) Cycling stability of Pt/$(RGO)_3$-$(Ti_3C_2T_x)_7$, Pt/RGO, Pt/$Ti_3C_2T_x$, Pt/CNT and Pt/C. 1000 consecutive cycle scans of methanol oxidation in 0.5 M H_2SO_4 and 0.5 M methanol obtained from (B) Pt/$(RGO)_3$-$(Ti_3C_2T_x)_7$, (C) Pt/RGO, (D) Pt/$Ti_3C_2T_x$, (E) Pt/CNT and (F) Pt/C catalysts, revealing the best cycling stability of Pt/$(RGO)_3$-$(Ti_3C_2T_x)_7$.

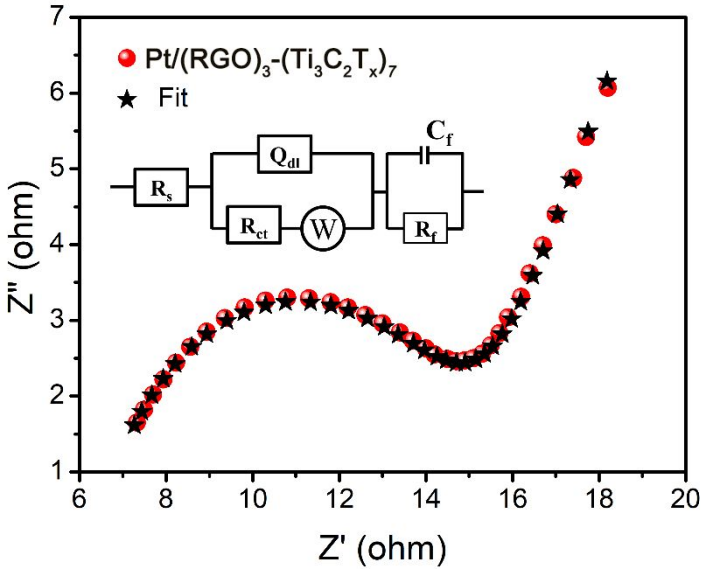

Figure S17. AC impedance spectrum of the Pt/RGO-$Ti_3C_2T_x$ electrode and the corresponding fitting curve, proving a good match between the testing and fitting results. The inset is the equivalent circuit: R_s and R_{ct} represent the resistances for electrolyte and catalyst, respectively, Q_{dl} is a constant phase element, W represents semiinfinite diffusion at the inte rface between electrolyte and electrode, R_f and C_f are the resistance and capacitance for the Nafion-carbon film, respectively.

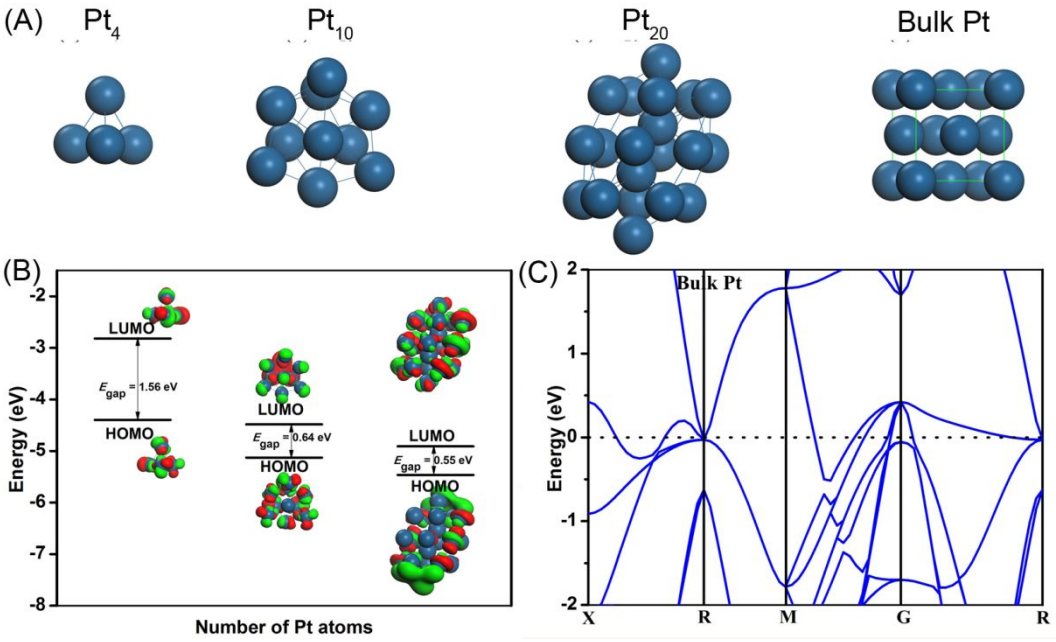

Figure S18. (A) The relaxed atomic structures for Pt_4, Pt_{10}, Pt_{20}, and bulk Pt. (B) The HOMO-LUMO gap for different Pt clusters and (C) the band structure of bulk Pt, demonstrating that the energy gaps of Pt nanoclusters increase with decreasing the particle size.

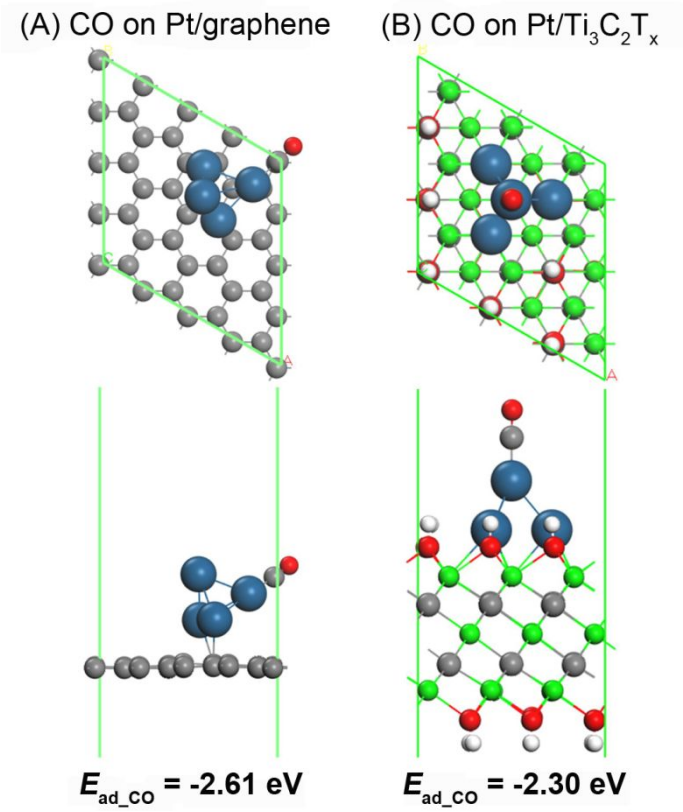

Figure S19. The relaxed atomic structures for the adsorption of CO on (A) Pt/graphene and (B) Pt/$Ti_3C_2T_x$, further confirming the stronger antipoisoning ability for Pt loaded on $Ti_3C_2T_x$ support.

Table S1. Compiled study comparing CV results for different catalysts.

Electrode	ECSA ($m^2\ g^{-1}$)	Mass activity ($mA\ mg^{-1}$)	Specific activity ($mA\ cm^{-2}$)
$Pt/(RGO)_9$-$(Ti_3C_2T_x)_1$	37.6	403.6	1.1
$Pt/(RGO)_7$-$(Ti_3C_2T_x)_3$	44.6	620.5	1.4
$Pt/(RGO)_5$-$(Ti_3C_2T_x)_5$	51.9	870.5	1.7
$Pt/(RGO)_3$-$(Ti_3C_2T_x)_7$	90.1	1102.0	1.2
$Pt/(RGO)_1$-$(Ti_3C_2T_x)_9$	72.5	929.5	1.3
$Pt/Ti_3C_2T_x$	32.0	158.4	0.5
Pt/RGO	35.4	305.6	0.9
Pt/CNT	27.5	155.1	0.6
Pt/C	24.6	110.8	0.5

Table S2. Comparison of methanol oxidation behavior on the $Pt/(RGO)_3$-$(Ti_3C_2T_x)_7$ composite and various Pt-based electrocatalysts.

Catalyst	ECSA ($m^2\ g^{-1}$)	Mass activity ($mA\ mg^{-1}$)	Scan rate ($mV\ s^{-1}$)	Electrolyte	Reference
$Pt/(RGO)_3$-$(Ti_3C_2T_x)_7$	90.1	1102.0	50	0.5 M H_2SO_4+ 0.5 M CH_3OH	This work
Pt/mesoporous carbon	N.A.	~450	20	0.5 M H_2SO_4 + 1 M CH_3OH	S1
Pt/macroporous carbon	N.A.	81.6	50	0.5 M H_2SO_4 + 0.5 M CH_3OH	S2
Pt/N-doped porous carbon	24.6	343.0	50	0.5 M H_2SO_4 + 1 M CH_3OH	S3
Pt/imidazolium-salt ionic liquid/CNT	67.6	`410.0	50	0.5 M H_2SO_4 + 0.5 M CH_3OH	S4
Pt/$[BMIM]BF_4$/ CNT	N.A	155.0	50	0.5 M H_2SO_4 + 1 M CH_3OH	S5
Pt/3D MoS_2-G	62.3	~91.8	10	1 M H_2SO_4 + 2 M CH_3OH	S6

Pt/3D C_3N_4-G	69.0	612.8	20	1 M H_2SO_4 + 2 M CH_3OH	S7
Pt/N-doped G	N.A.	~400.0	200	0.5 M H_2SO_4 +1 MCH_3OH	S8
Pt/N-doped G nanoribbon	64.6	~390.0	20	1 M H_2SO_4 + 2 M CH_3OH	S9
PtPd dendrites/G	81.6	647.2	50	0.5 M H_2SO_4 + 1 M CH_3OH	S10
PtPd dendrites	N.A.	490.0	50	0.5 M H_2SO_4 + 1 M CH_3OH	S11
AuPtCu nanowires	N.A.	~500.0	50	0.1 M $HClO_4$ + 1 M CH_3OH	S12
FePtPd nanowires	N.A.	488.7	50	0.1 M $HClO_4$ + 0.2 M CH_3OH	S13

Table S3. The charge-transfer resistance (R_{ct}) of different catalysts.

Electrode	R_{ct}	
	Value (ohm)	Error (%)
Pt/$(RGO)_3$-$(Ti_3C_2T_x)_7$	8.7	2.4
Pt/$Ti_3C_2T_x$	25.1	10.2
Pt/CNT	17.3	4.7
Pt/C	1268.0	1.9

References

(S1) Jiang, H.; Zhao, T.; Li, C.; Ma, J., Functional Mesoporous Carbon Nanotubes and Their Integration in Situ with Metal Nanocrystals for Enhanced Electrochemical Performances. *Chem. Commun.* **2011**, *47*, 8590-85922.

(S2) Bo, X.; Guo, L., Simple Synthesis of Macroporous Carbon–Graphene Composites and Their Use as a Support for Pt Electrocatalysts. *Electrochim. Acta* **2013**, *90*, 283–290.

(S3) Su, F.; Tian, Z.; Poh, C. K.; Wang, Z.; Lim, S. H.; Liu, Z.; Lin, J., Pt Nanoparticles Supported on Nitrogen-Doped Porous Carbon Nanospheres as an Electrocatalyst for Fuel Cells. *Chem. Mater.* **2010**, *22*, 832-839.

(S4) Guo, S.; Dong, S.; Wang, E., Constructing Carbon Nanotube/Pt Nanoparticle Hybrids Using an Imidazolium-Salt-Based Ionic Liquid as a Linker. *Adv. Mater.* **2010**, *22*, 1269-1272.

(S5) Chu, H.; Shen, Y.; Lin, L.; Qin, X.; Feng, G.; Lin, Z.; Wang, J.; Liu, H.; Li, Y., Ionic-Liquid-Assisted Preparation of Carbon Nanotube-Supported Uniform Noble Metal Nanoparticles and Their Enhanced Catalytic Performance. *Adv. Funct. Mater.* **2010**, *20*, 3747-3752.

(S6) Gao, Z.; Li, M.; Wang, J.; Zhu, J.; Zhao, X.; Huang, H.; Zhang, J.; Wu, Y.; Fu, Y.; Wang, X., Pt Nanocrystals Grown on Three-Dimensional Architectures Made from Graphene and MoS_2 Nanosheets: Highly Efficient Multifunctional

Electrocatalysts toward Hydrogen Evolution and Methanol Oxidation Reactions. *Carbon* **2018**, *139*, 369-377.

(S7) Huang, H.; Yang, S.; Vajtai, R.; Wang, X.; Ajayan, P. M., Pt-Decorated 3D Architectures Built from Graphene and Graphitic Carbon Nitride Nanosheets as Efficient Methanol Oxidation Catalysts. *Adv. Mater.* **2014**, *26*, 5160-5165.

(S8) Xiong, B.; Zhou, Y.; Zhao, Y.; Wang, J.; Chen, X.; O'Hayre, R.; Shao, Z., The Use of Nitrogen-Doped Graphene Supporting Pt Nanoparticles as a Catalyst for Methanol Electrocatalytic Oxidation. *Carbon* **2013**, *52*, 181–192.

(S9) Huang, H.; Ye, G.; Yang, S.; Fei, H.; Tiwary, C. S.; Gong, Y.; Vajtai, R.; Tour, J. M.; Wang, X.; Ajayan, P. M., Nanosized Pt Anchored onto 3D Nitrogen-Doped Graphene Nanoribbons Towards Efficient Methanol Electrooxidation. *J. Mater. Chem. A* **2015**, *3*, 19696-19701.

(S10) Guo, S.; Dong, S.; Wang, E., Three-Dimensional Pt-on-Pd Bimetallic Nanodendrites Supported on Graphene Nanosheet: Facile Synthesis and Used as an Advanced Nanoelectrocatalyst for Methanol Oxidation. *Acs Nano* **2010**, *40*, 547–555.

(S11) Wang, L.; Nemoto, Y.; Yamauchi, Y., Direct Synthesis of Spatially-Controlled Pt-on-Pd Bimetallic Nanodendrites with Superior Electrocatalytic Activity. *J. Am. Chem. Soc.* **2011**, *133*, 9674–9677.

(S12) Hong, W.; Wang, J.; Wang, E., Dendritic Au/Pt and Au/PtCu Nanowires with Enhanced Electrocatalytic Activity for Methanol Electrooxidation. *Small* **2014**, *10*, 3262–3265.

(S13) Guo, S.; Zhang, S.; Sun, X.; Sun, S., Synthesis of Ultrathin FePtPd

Nanowires and Their Use as Catalysts for Methanol Oxidation Reaction. *J. Am. Chem. Soc.* **2011**, *133*, 15354–15357.